Stacking of the square-lattice antiferromagnetic planes in $Ca_2CuO_2Cl_2$

D. Vaknin, L. L. Miller, and J. L. Zarestky
Ames Laboratory and Department of Physics and Astronomy, Iowa State University, Ames, Iowa 50011
(Received 5 December 1996; revised manuscript received 15 May 1997)

Single-crystal neutron elastic and quasielastic scattering and magnetization studies of the spin-$\frac{1}{2}$ square-lattice Heisenberg antiferromagnet $Ca_2CuO_2Cl_2$ indicate an unusual stacking of the antiferromagnetic planes in the Néel state ($T_N=247\pm5$ K) which is different from the collinear stacking in isostructural $Sr_2CuO_2Cl_2$. A generalized magnetic model is presented to describe the data. Elastic scattering along the $(\frac{1}{2}\frac{1}{2}l)$ rod is observed above T_N, suggesting that the CuO_2 planes, although uncoupled, maintain some degree of two-dimensional order up to a crossover temperature ($T_{co}\approx280$ K) to the isotropic Heisenberg state. No structural phase transition from the $I4/mmm$ symmetry was observed in the temperature range 10–300 K. [S0163-1829(97)09437-X]

I. INTRODUCTION

Insight into the pairing mechanism of high-temperature superconductors (HTSC's) is being sought by studying the parent compounds which are generally undoped antiferromagnetic insulators. La_2CuO_4 is one of the simplest superconducting parent compounds and contains what many believe are two of the salient structural features of HTSC's, namely, square-lattice sheets of CuO_2 and Cu-O distances $\simeq$1.9 Å. Insulating La_2CuO_4 (Ref. 1) is tetragonal at high temperatures and has strong, intraplanar, oxygen-mediated antiferromagnetic (AF) superexchange coupling (J) between the localized Cu^{2+} spins which gives rise to two-dimensional (2D) dynamic magnetic short-range order below a temperature $T\sim J\simeq1400$ K. The system exhibits collinear 3D magnetic long-range order (LRO) below $T_N\simeq320$ K. La_2CuO_4 is orthorhombic below $\simeq$530 K, and the distortion associated with it brings about weak ferromagnetism of the Dzyaloshinsky-Moriya type. Neither the covalently bonded apical oxygen atoms nor the orthorhombic distortion are common to all HTSC's, and they create undesired complications. Simpler model systems, such as members of the series $M_2CuO_2X_2$ (M=Ca, Sr, Ba; X=F, Cl, Br), are therefore being examined as model systems for undoped state of the single-CuO_2-plane HTSC's.

Studies[2,3] on $Sr_2CuO_2Cl_2$ show it to be insulating and tetragonal ($I4/mmm$) to at least 10 K with room-temperature Cu-O distances of 1.99 Å and strong in-plane Cu-O-Cu superexchange interactions ($J\simeq1500$ K, Ref. 4). Compared to La_2CuO_4, the interplanar distances are greater and the apical oxygen atoms are replaced with the more ionic chlorine. The interplanar superexchange interaction (J') is consequently weak or nonexistent, and other causes of 3D ordering are being sought. Below the 3D ordering at $T_N\simeq255$ K, the spins are oriented antiferromagnetically in the CuO_2 plane with the spin planes stacked collinearly. $Sr_2CuO_2Cl_2$ is not only a good model system for the single-plane cuprates, it is also a very good spin-$\frac{1}{2}$, 2D square lattice quantum Heisenberg antiferromagnet (2DSLQHA) against which theories are being tested.

The 2D Heisenberg behavior of the cuprates above T_N stems from the very large isotropic 2D intraplanar coupling constant. Comparisons between experimental measurements of the correlation lengths in La_2CuO_4,[5,6] $Sr_2CuO_2Cl_2$,[7] and Pr_2CuO_4,[8] with the 2D quantum nonlinear sigma model[9] (QNLσM) or Monte Carlo calculations,[10] show reasonably good agreement. Originally, the Heisenberg behavior was thought to apply over nearly the entire T_N to $T\sim J$ range. Near T_N, the XY and Ising anisotropies and the interplanar interactions would become relatively important and induce 3D ordering. A recently discovered crossover in the spin dimensionality from the 2D Heisenberg to a 2D XY-like or Ising-like behavior in $Sr_2CuO_2Cl_2$ (Refs. 11 and 12) shows that one or more of the anisotropies sets in at a much higher temperature. The relative magnitudes of the various interaction energies are not well understood, even for this simple compound. Studies of other members of the $M_2CuO_2X_2$ series are desirable because the small differences (e.g., electronegativity, mass, radii) can, as shown below, produce dramatic changes which might elucidate important interactions in the single-plane cuprates.

$Ca_2CuO_2Cl_2$ is isostructural with $Sr_2CuO_2Cl_2$ (Ref. 13) and displays similar electronic band structure[14,15] and other properties with a few notable exceptions. The room-temperature interplanar distances for $Sr_2CuO_2Cl_2$, $Ca_2CuO_2Cl_2$, and La_2CuO_4 are 7.81, 7.54, and 6.58 Å and the Cu-O distances are 1.99, 1.94, and 1.90 Å, respectively.[3] This makes the $Ca_2CuO_2Cl_2$ lattice and Cu-O distances correspond better with those of La_2CuO_4, which leads one to expect more similar interaction strengths and behavior. Also, whereas $Sr_2CuO_2Cl_2$ has yet to be doped,[2] $Ca_2CuO_2Cl_2$ becomes a HTSC when doped at high pressures,[16] and thus studies of stoichiometric $Ca_2CuO_2Cl_2$ could be more representative of the undoped state of the HTSC's. Additionally, $Sr_2CuO_2Cl_2$ has a collinear stacking of the AF CuO_2 planes oriented in the [110] crystallographic direction (and equivalent domains with spins along [110], giving rise to a $\sqrt{2}\times\sqrt{2}\times1$ magnetic cell, as is the case in most insulating cuprates.[3,17,18] $Ca_2CuO_2Cl_2$, however, has a $\sqrt{2}\times\sqrt{2}\times2$ magnetic cell which requires a different stacking of the magnetic lagers. The primary subject of this report lies in the magnetic structure below and just above T_N.

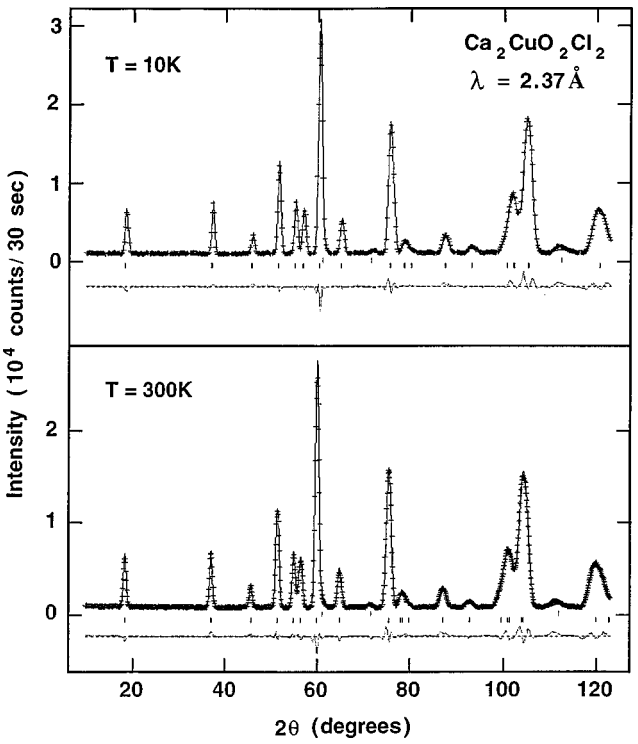

FIG. 1. Powder diffraction patterns at 10 and 300 K of $Ca_2CuO_2Cl_2$. The solid lines are fits to the data using the $I4/mmm$ structural parameters in Table I; the lower dashed line is the difference between the measured (+ symbols) and the fitted curve. The fit accounts for reflections of the polycrystalline aluminum sample container.

II. EXPERIMENTAL DETAILS AND RESULTS

A. Elastic magnetic neutron scattering

Neutron-scattering measurements were carried out on the HB-1A triple-axis spectrometer at the High Flux Isotope Reactor (HFIR) at Oak Ridge National Laboratory. A monochromatic neutron beam of wavelength $\lambda=2.357$ Å ($k_i=2\pi/\lambda=2.666$ Å^{-1}; $\mathbf{k}_i$ and $\mathbf{k}_f$ denote the incoming and outgoing wave vectors, respectively) was selected by a double-monochromator system using the (002) Bragg reflection of highly oriented pyrolytic graphite (HOPG) crystals. The $\lambda/2$ component in the beam was removed (to better than 1.3 parts in 10^4) by a set of HOPG crystals situated between the two monochromating crystals. The sample crystal was wrapped in thin Al foil and loaded into an Al can (under He atmosphere), which was then mounted in a Displex cryostat for measurements. The collimating configuration used was 40′, 40′, *S*, 34′, 68′.

The $Ca_2CuO_2Cl_2$ single crystal used in the present neutron scattering investigation was grown from a molten flux of 60% $Ca_2CuO_2Cl_2$ (prepared as in Ref. 2) and 40% $CaCl_2$ by slow cooling the molten charge from 900 °C in an alumina crucible. A single crystal, of approximate dimensions $0.5\times0.5\times0.05$ cm^3, with a mosaic spread of 2.0° was selected for the neutron studies. A polycrystalline sample from the same batch was ground for neutron-powder-diffraction structural studies to examine the quality of the sample. Figure 1 shows neutron powder diffraction patterns at 10 and 300 K. The crystal structure at the two temperatures can be described by the same $I4/mmm$ space group. The structure was refined by using the Rietveld method with the GSAS program.[19] The structural parameters obtained from fitting the data to the K_2NiF_4-type structure are listed in Table I.

TABLE I. Structural parameters of $Ca_2CuO_2Cl_2$ at $T=10$ K and at $T=300$ K obtained from the diffraction data shown in Fig. 1. The model structure has $I4/mmm$ symmetry with the following generating atomic positions: Cu at the origin (000), O at $(0\frac{1}{2}0)$, and Ca and Cl at $(00Z)$.

T (K)	a (Å)	c (Å)	Z_{Ca}	Z_{Cl}
10	3.8673(5)	14.9567(25)	0.39549(40)	0.18325(20)
300	3.8745(4)	15.0758(16)	0.39644(24)	0.18222(12)

Detailed neutron-diffraction studies of the powder (28 g) at $T=10$ K in specific regions of reciprocal space showed no evidence of extra reflections that in general signify structural or magnetic phase transitions. Weak signals are difficult to detect even with a large volume of powdered sample due to the fact that the scattering is distributed over the Debye-Scherrer cone and the background level is relatively much higher than that expected from a single crystal. In fact, neutron-diffraction studies below ≈250 K with single-crystal $Ca_2CuO_2Cl_2$ revealed a new set of very weak reflections that could be indexed based on the crystallographic unit cell as $(h/2\ h/2\ l/2)$ where h and l are odd integers. Figure 2 shows scans along the $(\frac{1}{2}\frac{1}{2}l)$ and $(\frac{3}{2}\frac{3}{2}l)$ lines in reciprocal space. The intensities of the magnetic reflections shown in Fig. 2 are on the order of 0.1% of the nuclear (110) or (006) Bragg reflections. The temperature dependence of the integrated intensity of the $(\frac{1}{2}\frac{1}{2}\frac{1}{2})$ reflection, shown in Fig. 3, indicates that a phase transition occurs at $T=247\pm5$ K.The significant difference in intensity between the $(\frac{1}{2}\frac{1}{2}l)$ and $(\frac{3}{2}\frac{3}{2}l)$ reflections is consistent (as will be shown quantitatively below) with the reduction in intensity due to the magnetic form factor of Cu^{2+}, suggesting that these new reflections are antiferromagnetic in origin. This conclusion is consistent with $T_N=260\pm5$ K found by Mössbauer spectroscopy.[20] Notice the absence of the $(\frac{1}{2}\frac{1}{2}0)$ peak, a characteristic and dominant magnetic reflection in $Sr_2CuO_2Cl_2$ and in the analogous distorted La_2CuO_4.

In order to quantitatively describe the data, we choose two specific models (Fig. 4) which can be derived from a generalized magnetic unit cell. The planar magnetic moments have antiparallel nearest-neighbor (NN) orientations within each CuO_2 plane analogous to the in-plane ordering of $Sr_2CuO_2Cl_2$and La_2CuO_4. Only a single orientation angle θ_l is required for each plane l to define the in-plane spin directions. In the generalized model every other plane is coupled in an antiparallel fashion to obtain the observed magnetic unit cell having twice the length along the c axis as the crystallographic unit cell. The even numbered planes in Fig. 4 have angles $\theta_0, \theta_0+\pi, \theta_0, \theta_0+\pi, \ldots$, and the odd numbered planes have angles $\theta_1, \theta_1+\pi, \theta_1, \theta_1+\pi, \ldots$ with no relationship between θ_0 and θ_1 at this point. Two simple models based on this generalized magnetic cell have either *collinear* ($\theta_0+\theta_1=0$ or π) or *noncollinear* ($\theta_0+\theta_1=\pm\pi/2$) stacking. The collinear arrangement (Fig. 4, right) can be constructed by doubling the magnetic unit cell of $Sr_2CuO_2Cl_2$ with equivalent spins in the two magnetic unit cells antiparallel. This arrangement gives rise to two domains

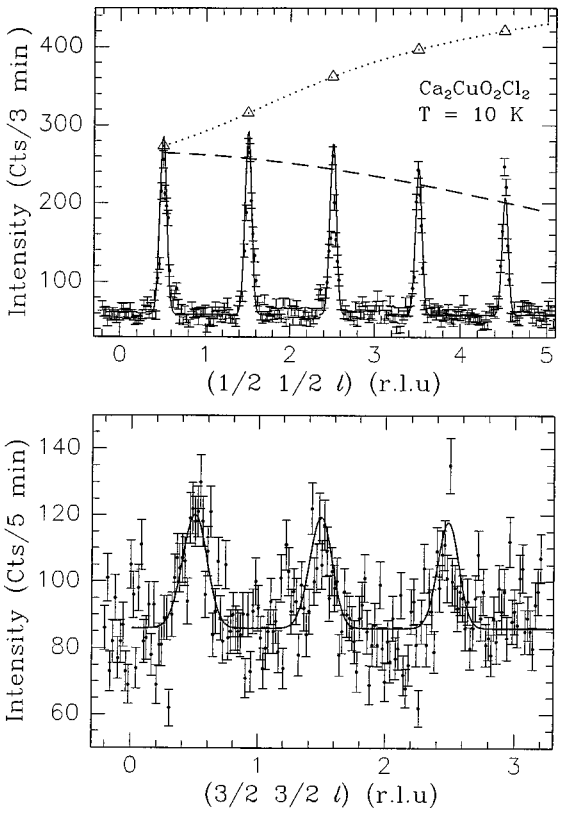

FIG. 2. Scans along the $(\frac{1}{2}\frac{1}{2}l)$ (upper panel) and along the $(\frac{3}{2}\frac{3}{2}l)$ using the $I4/mmm$ reciprocal space indices notation (rlu stands for reciprocal lattice unit, $c^*=2\pi/c$). Notice the absence of the $(\frac{1}{2}\frac{1}{2}0)$ magnetic peak which is typical for the single plane insulating and AF cuprates. The solid lines are calculated from the magnetic models as described in the text. The dashed line corresponds to the calculated magnetic form factor squared for Cu^{2+}, and the triangles (connected with dotted line) are the calculated moduli of the magnetic structure factor squares [Eqs. (3) and (4)].

which are accounted for in the derivation below. The noncollinear model (Fig. 4, left) is such that the orientation of the spins changes by an angle of 90° in a helical fashion on passing from one CuO_2 plane to the next along the c axis,

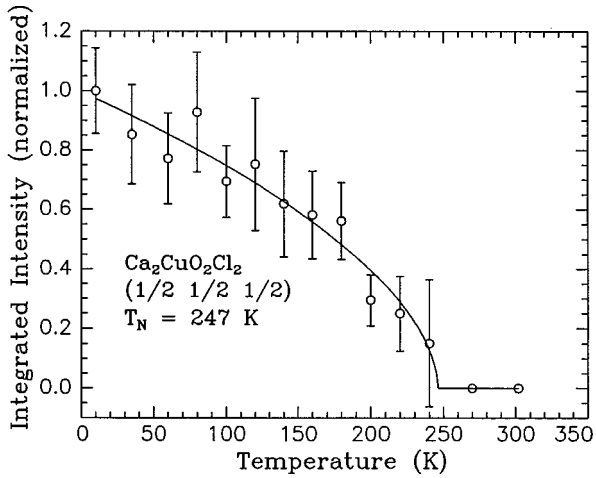

FIG. 3. Temperature dependence of the integrated intensity of the $(\frac{1}{2}\frac{1}{2}\frac{1}{2})$ magnetic reflection indicating an antiferromagnetic long range order transition at $T_N \simeq 247$ K.

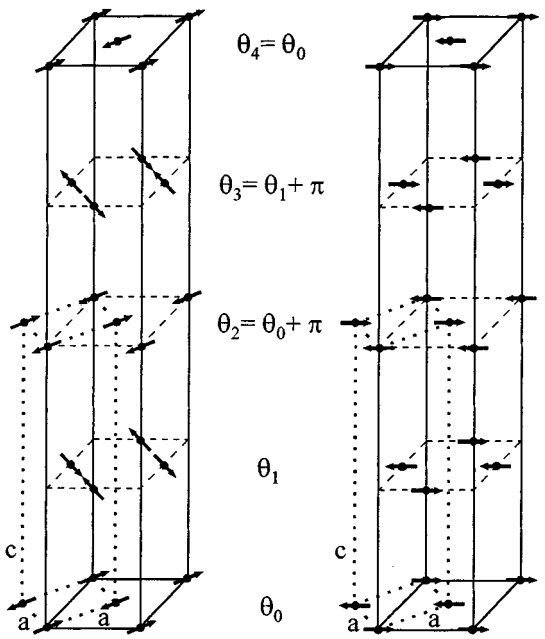

FIG. 4. Two special cases of the proposed general model describing the Cu^{2+} spin arrangement in the $Ca_2CuO_2Cl_2$ magnetic unit cell. Angles θ_l indicate planar orientation of the spin planes relative to the crystallographic a axis. The angles θ_0 and $\theta_0+\theta_1$ are unspecified in the general model. Left: noncollinear helical model with $\theta_0+\theta_1=\pi/2$. Right: collinear model with $\theta_0+\theta_1=0$. θ_0 chosen as 0 and $\pi/2$ for helical and collinear models, respectively, to maintain consistency with dipolar calculations described in the text. The crystallographic unit cell is drawn with a dotted line.

forming either right- or left-handed helical domains. The advantage of the helical model is that the relationship between adjacent layers does not vary, whereas other models, including the collinear one presented here, are such that they necessitate at least two types of nearest-neighbor arrangements.

The intensity of a magnetic Bragg reflection for a given reciprocal lattice vector $\boldsymbol{\tau}=\mathbf{Q}$ $[\mathbf{Q}=\mathbf{k}_i-\mathbf{k}_f$, $\tau=2k_i\sin(\phi_B/2)$, and ϕ is the scattering angle] is given by[21,22]

$$I_M(\boldsymbol{\tau})=\frac{A[r_0\mu f(\boldsymbol{\tau})\mathbf{F}_M(\boldsymbol{\tau})]^2}{\sin(\phi_B)}, \tag{1}$$

where A is a scale factor that can be determined from Bragg reflections arising from nuclear scattering in the same crystal, $r_0=0.269\times10^{-12}$ cm, μ is the magnitude of the magnetic moment in units of μ_B, and $f(\mathbf{Q})$ is the magnetic form factor of Cu^{2+} (Ref. 23). The magnetic structure factor $\mathbf{F}_M(\boldsymbol{\tau})$ is given by

$$\mathbf{F}_M(\boldsymbol{\tau})=\sum_{i=1}^{N} e^{i\boldsymbol{\tau}\cdot\mathbf{R}_i}[\hat{\boldsymbol{\tau}}\times(\hat{\boldsymbol{\mu}}\times\hat{\boldsymbol{\tau}})], \tag{2}$$

where $\mathbf{R}_i$ is the position of the magnetic moment i pointing in the direction of the unit vector $\hat{\boldsymbol{\mu}}_i$ and $\hat{\boldsymbol{\tau}}$ is a unit vector in the direction of the magnetic reciprocal lattice vector $\boldsymbol{\tau}$ (or the scattering vector $\mathbf{Q}$).

Carrying out the summation in Eq. (2) for the collinear model in terms of the $\hat{h}$, $\hat{k}$, and $\hat{l}$ unit vectors of the magnetic unit cell yields

$$\mathbf{F}_M(\boldsymbol{\tau}) = 2\sin\left(\frac{\pi l}{2}\right)[e^{i\pi k} - e^{i\pi h} + e^{i\pi l/2}(1 - e^{i\pi(h+k)})]\sin\alpha, \tag{3}$$

where α is the angle between the moment $\boldsymbol{\mu}$ and the scattering vector $\mathbf{Q}$. This summation is performed using h, k, and l indices that correspond to the magnetic unit cell (lattice constants $a_M = \sqrt{2}$, $c_M = 2c$). For example, with this notation the $(\frac{1}{2}\frac{1}{2}\frac{1}{2})$ point defined on the crystallographic unit cell corresponds to $(101)_M$.

Similar calculations for the noncollinear model yield

$$\mathbf{F}_M(\boldsymbol{\tau}) = \left[\frac{(h^2-\gamma^2)}{\gamma^2} f_1 + \frac{hk}{\gamma^2} f_2\right]\hat{h} + \left[\frac{hk}{\gamma^2} f_1 + \frac{(k^2-\gamma^2)}{\gamma^2} f_2\right]\hat{k} + \left[\frac{hka/c}{\gamma^2} f_1 + \frac{kla/c}{\gamma^2} f_2\right]\hat{l}, \tag{4}$$

where

$$f_1 = 4\sin\left(\frac{\pi l}{2}\right)\sin\left(\frac{\pi(h+k)}{2}\right)e^{i\pi(h+k+l)/2},$$

$$f_2 = 4\sin\left(\frac{\pi l}{2}\right)\sin\left(\frac{\pi(h-k)}{2}\right)e^{i\pi(h+k)/2},$$

and

$$\gamma^2 = h^2 + k^2 + l^2\left(\frac{a}{c}\right)^2.$$

It is interesting to note that the moduli of the magnetic structure factor squared $|\mathbf{F}_M(\boldsymbol{\tau})|^2$, for $(\frac{1}{2}\frac{1}{2}l)$ $[(10l)_M]$ reflections are identical for the two models assuming appropriate weights due to the domain formation in the collinear model. Therefore, from the set of reflections reported here alone, it is impossible to distinguish between the two models. The calculations for these reflections are shown as triangles in Fig. 2 with arbitrary units. The gradual increase of the moduli squared as l becomes larger is due to the increase in angle between the magnetic moment in the plane and the scattering vector $\mathbf{Q}$. This increase of $|\mathbf{F}_M(\boldsymbol{\tau})|^2$ compensates for the expected fall off of intensity due to the form factor of Cu^{2+}, $f(\mathbf{Q})$ (shown, not to scale, as dashed line in Fig. 2).[23] Using Eqs. (1)–(4) and a scale factor A that was determined from nuclear Bragg reflections, the data can be fitted with four adjustable parameters—a constant background, the magnitude of the magnetic moment μ, and two global peak-shape parameters. The shape of the magnetic Bragg reflections was taken to be Gaussian of width Δ that varies linearly with Q over the ranges shown in Fig. 2 as $\Delta(Q) = \Delta_0 + \Delta_1 Q$. The average staggered magnetic moment obtained from the best fit is $\mu = (0.25 \pm 0.1)\mu_B$ at $T = 10$ K. This is lower than theoretical calculations predict for the 2DSLQHA model,[24] but comparable in size to the values found for the isostructural $Sr_2CuO_2Cl_2$.

The disappearance of the $(\frac{1}{2}\frac{1}{2}\frac{1}{2})$ magnetic reflection above T_N was followed by a gradual decrease in the *apparent* background. The backgroundlike scattering at 270 K was significantly larger than at 300 K suggesting that some degree of 2D static order is preserved above the 3D AF transition and below ≈300 K. In general, the Bragg condition for diffraction from an ideal 2D system is independent of the component of the scattering vector normal to the 2D plane, $\mathbf{Q}_\perp$, so that $\mathbf{Q} = \boldsymbol{\tau}_{2D} + \mathbf{Q}_\perp$, where $\boldsymbol{\tau}_{2D}$ is the 2D reciprocal lattice vector. The scattering from an ordered 2D system is thus characterized by a *rod* of scattering normal to the 2D plane. Assuming that above T_N the CuO_2 planes decouple but preserve some degree of in-plane magnetic order with no correlations between planes, a rod of scattering (consisting of the superposition of rods from all the planes and superimposed on the background scattering) along $(\frac{1}{2}\frac{1}{2}l)$ is expected.

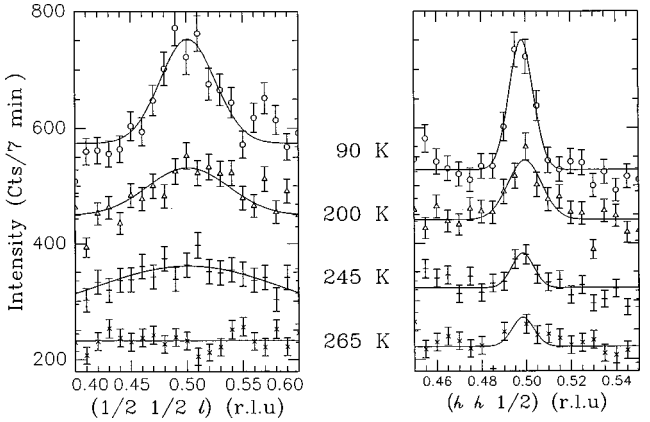

FIG. 5. $(h/2\ h/2\ l/2)$ scans along (left panel) and across (right panel) the 2D rod at various temperatures (scans are shifted by a constant intensity for clarity). The broadening and the loss of a sharp peak along the rod above T_N and the sharp peak across the rod indicate that some degree of 2D static order is preserved above $T_N \simeq 247$ K.

Figure 5 shows scans along and across the l rod. At temperatures above 245 K the *sharp* reflection along the rod broadens and disappears while in the transverse scan it persists. The broadening of the scan along the l direction is evidence for the loss of correlation between planes. A transverse scan across the rod and its temperature dependence might help determine the spin dimensionality of the system (Ising-like or higher). If the transverse scan across the rod is resolution limited, this would establish that the system has true 2D order; i.e., it is in an Ising-like state. Other states, with peaks that are broader than the resolution will necessitate a complete temperature dependence and/or polarized neutron beam technique to be classified properly. Although the experimental transverse scans shown in Fig. 5 above T_N are sharp and suggest some degree of static ordering, the count rate of the signals is too poor to unequivocally establish that they are indeed resolution-limited above T_N. This point can be clarified with the availability of larger single crystals with improved signal-to-noise ratio.

Figure 6 shows integrated intensities of elastic scans along the $(\frac{1}{2}\frac{1}{2}l)$ rod versus temperature near $(\frac{1}{2}\frac{1}{2}\frac{1}{2})$. Above T_N, the fixed-range integrated intensities drop linearly with increasing temperature, intercepting the background at ≈280 K. We suggest that this is the crossover temperature ($T_{co} \approx 280$ K) from the low spin symmetry (i.e., XY-like or Ising-like) to a higher-temperature isotropic Heisenberg-like behavior. Above the crossover temperature the system is expected to posses strongly fluctuating correlated domains.[25]

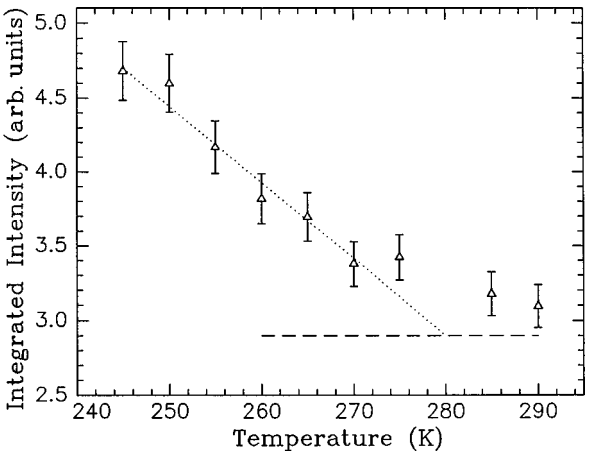

FIG. 6. Temperature dependence of the integrated intensity of the $(\frac{1}{2}\frac{1}{2}\frac{1}{2})$ reflection along the 2D rod, indicating a possible crossover to a more isotropic spin state above ≈280 K. Background level at 300 K is shown with a dashed line.

These should be observed with the inelastic or quasielastic scattering as described below. This is consistent with recent observations[11,12] of a crossover from Heisenberg to *XY*-like (or lower spin dimensionality) up to 50 K above the 3D AF ordering in $Sr_2CuO_2Cl_2$.

B. Quasielastic magnetic neutron scattering

The scattering geometry for the quasielastic scattering measurements is shown in Fig. 7, where a two-axis configuration with no energy analyzer was used. Scans, like the ones shown in Fig. 8(a) below, are so-called ϕ scans (ϕ is the scattering angle), which maintain the *c* axis (**c**) of the sample antiparallel to the outgoing beam. The geometry is similar to the one reported in Ref. 26 where one practically integrates over a wide range of energies due to fluctuations in a 2D magnetic system.

In general, the partial differential cross section for scattering neutrons from a magnetic spin system with a dynamic structure factor $S^{\alpha\alpha}(\mathbf{Q},\omega)$ into a solid angle element $d\Omega$ is given by[27]

$$\frac{d^2\sigma}{d\Omega dE_f} = A(\mathbf{Q})\frac{k_f}{k_i}\sum_{\alpha}\left(1-\frac{Q_\alpha^2}{Q^2}\right)S^{\alpha\alpha}(\mathbf{Q},\omega), \qquad (5)$$

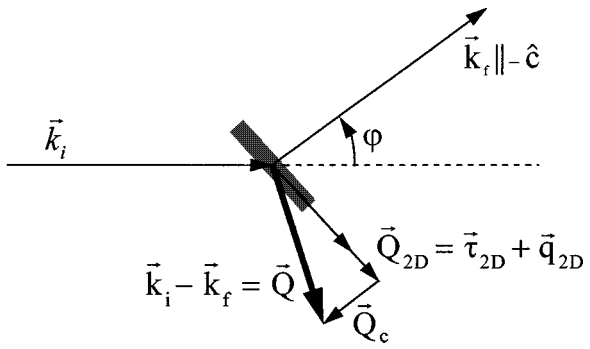

FIG. 7. Illustration of the quasielastic neutron scattering geometry described in the text.

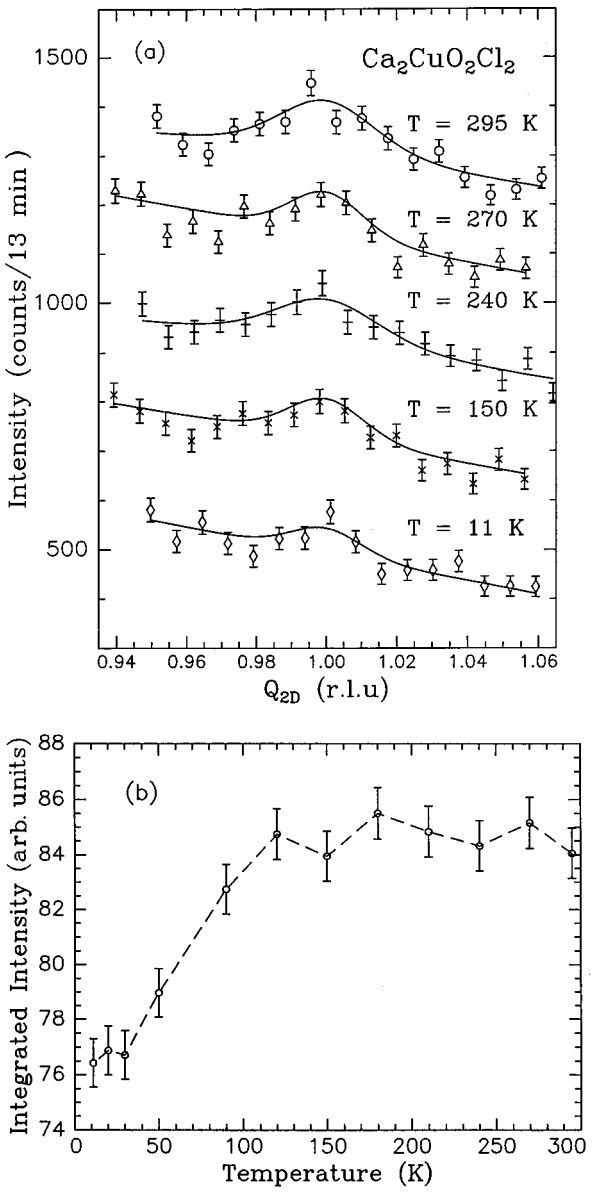

FIG. 8. (a) Quasielastic 2D neutron scattering intensity from $Sr_2CuO_2Cl_2$ vs $Q_{2D}=h\tau_{2D}$ at different temperatures as indicated (constant added for clarity). A reciprocal lattice unit (rlu) is $\tau_{2D}=\sqrt{2}\pi/a=1.149$ Å^{-1}. The solid lines are nonlinear least-squares fits to Lorentzians [Eq. (13)]. (b) Integrated intensity vs temperature of the 2D quasielastic scattering.

where the axes $\alpha=x,y,z$ and the incoming and outgoing neutron energies and wave vectors are E_i, E_f and $\mathbf{k}_i$, $\mathbf{k}_f$, respectively. The energy and momentum transfers to the sample are $\hbar\omega=E_i-E_f$ and $\mathbf{Q}=\mathbf{k}_i-\mathbf{k}_f$, respectively. The function $A(\mathbf{Q})$ contains the square of the atomic magnetic form factor $f(\mathbf{Q})$, the Debye-Waller factor $\exp[2W(\mathbf{Q})]$, and physical constants. Using the fact that $E=\hbar^2k^2/2m_n$, where m_n is the neutron mass, one can solve for the ratio k_f/k_i in Eq. (5) in terms of E_i and ω: $k_f/k_i=\sqrt{1-\hbar\omega/E_i}\equiv\sqrt{1-r}$, where $r\equiv\hbar\omega/E_i$ is the ratio of the energy transfer to the incident neutron energy (r is positive for neutron energy loss processes and negative for neutron energy gain). Then Eq. (5) becomes

$$\frac{d^2\sigma}{d\Omega dE_f}=A(\mathbf{Q})\sqrt{1-r}\sum_{\alpha}\left(1-\frac{Q_\alpha^2}{Q^2}\right)S^{\alpha\alpha}(\mathbf{Q},\omega). \quad (6)$$

This is a useful form of Eq. (5) for experiments in which E_i is fixed, as are those reported on here.

The dynamic structure factor $S^{\alpha\alpha}(\mathbf{Q},\omega)$ in Eqs. (5) and (6) is the space and time Fourier transform of the correlation function between spins at positions $\mathbf{0}$ and $\mathbf{R}$:

$$S^{\alpha\alpha}(\mathbf{Q},\omega)=\frac{1}{2\pi}\sum_{R} e^{iQ\cdot R}\int_{-\infty}^{\infty}e^{i\omega t}\langle S^{\alpha}(\mathbf{0},0)S^{\alpha}(\mathbf{R},t)\rangle dt. \quad (7)$$

For a 2D spin system with no interplanar correlations, from Eq. (7), $S^{\alpha\alpha}(\mathbf{Q},\omega)$ only depends on the component $\mathbf{Q}_{2D}$ of $\mathbf{Q}$ in the 2D (a-b) plane and is independent of the component $\mathbf{Q}_c$ perpendicular to the 2D plane and therefore

$$\mathbf{Q}=\mathbf{Q}_{2D}+\mathbf{Q}_c, \quad (8)$$

as shown in Fig. 7. Since $S^{\alpha\alpha}(\mathbf{Q},\omega)$ is independent of $\mathbf{Q}_c$, the magnetic scattering forms rods in reciprocal space parallel to $\mathbf{c}^*$, passing through the 2D magnetic reciprocal lattice points $\boldsymbol{\tau}_{2D}$ in the $\mathbf{a}^*$-$\mathbf{b}^*$ plane. From the scattering geometry in Fig. 7, in which the outgoing beam is antiparallel to $\mathbf{c}$, one has

$$Q_{2D}=k_i\sin\phi, \quad (9a)$$

$$Q_c=k_f-k_i\cos\phi=k_i(\sqrt{1-r}-\cos\phi), \quad (9b)$$

$$Q^2=k_i^2(2-r-2\sqrt{1-r}\,\cos\phi). \quad (9c)$$

Note that although $S^{\alpha\alpha}(\mathbf{Q},\omega)$ is independent of $\mathbf{Q}_c$ from Eq. (9c), Q_c does depend on the energy transfer $\hbar\omega$. $\mathbf{Q}_{2D}$ decomposes according to

$$\mathbf{Q}_{2D}=\mathbf{q}_{2D}+\boldsymbol{\tau}_{2D}, \quad (10)$$

where $\mathbf{q}_{2D}$ is the deviation of $\mathbf{Q}_{2D}$ from the (nearest) 2D magnetic reciprocal lattice vector $\boldsymbol{\tau}_{2D}$.

Since this neutron scattering experiment keeps E_i (and hence k_i) fixed, from Eq. (9a), the scattering geometry in Fig. 7 has the important feature that the momentum transfer Q_{2D} to the spin system is independent of energy transfer $\hbar\omega$. Thus, in a two-axis experiment with no energy analyzer as in Fig. 7, an almost perfect energy integration over the 2D dynamic structure function is performed at each Q_{2D} from $r=1$ ($E_f=0$ meV) to $r\sim-4$ ($E_f\sim60$ meV; this cutoff is mainly due to the magnetic form factor). Thus the dominant low-energy ($|r|<1$) fluctuations are properly included within the range of integration.[25,26,28] Integrating $S^{\alpha\alpha}(\mathbf{Q},\omega)$ [Eq. (7)] over ω yields the intensity[25–28]

$$I(\mathbf{Q})\sim\frac{d\sigma}{d\Omega}\approx A(\mathbf{Q})\sum_{\alpha}\left(1-\frac{Q_2^{\alpha}}{Q^2}\right)S^{\alpha\alpha}(\mathbf{Q}_{2D}), \quad (11)$$

where

$$S^{\alpha\alpha}(\mathbf{Q}_{2D})=\int_{-\infty}^{\infty}S^{\alpha\alpha}(\mathbf{Q}_{2D},\omega)d\omega=\sum_{R} e^{i\mathbf{Q}_{2D}\cdot R}\langle S^{\alpha}(\mathbf{0})S^{\alpha}(\mathbf{R})\rangle \quad (12)$$

is the static (equal-time) scattering function.

Quasielastic scattering scans were made with $\mathbf{Q}$ in the $[hh0]$-$[00l]$ reciprocal lattice plane, using the geometry in Fig. 7, across the $(\frac{1}{2}\frac{1}{2}l)$ (in crystallographic reciprocal lattice units) magnetic scattering rod of the 2D Cu^{2+} spin-$\frac{1}{2}$ square lattice of $Ca_2CuO_2Cl_2$ with lattice constant $a=3.867$ Å. Thus $\mathbf{Q}_{2D}$, $\mathbf{q}_{2D}$, and $\boldsymbol{\tau}_{2D}$ in Fig. 7 are collinear. Incident neutrons of fixed energy $E_i=14.725$ meV were used. The length of the 2D AF reciprocal lattice vector is $\tau_{2D}=\sqrt{2}\pi/a=1.149$ Å^{-1} [defined here as a ''reciprocal lattice unit'' (rlu)]. The condition on the scattering angle ϕ in Fig. 7 for the center of the scan is, using Eq. (9a), $\tau_{2D}=Q_{2D}=k_i\sin\phi$, yielding $\phi=25.53°$. According to Eq. (9b), the value of l depends both on the energy transfer and on ϕ: $l=Q_c/(2\pi/c)$, where $c=14.957$ Å; for $\hbar\omega=0$, $l=0.620$ at the center of the scan.

Figure 8(a) shows representative energy-integrated two-axis scans at various temperatures. The peaks were each fitted to a linear function background plus a Lorentzian form[7]

$$S(q_{2D})=\frac{S(0)}{1+q_{2D}^2/\kappa^2}, \quad (13)$$

convoluted with the resolution function of the instrument. $\kappa\equiv\xi^{-1}$ is the inverse 2D AF correlation length. The quality of the data in Fig. 8(a) yields large uncertainties on the values of κ as a function of temperature from which only approximate values for κ are extracted. Above T_N, $\kappa\approx0.01$ Å^{-1}, whereas below T_N, $\kappa\approx0.003$ Å^{-1}. Figure 8(b) shows the temperature dependence of the Q-integrated intensities of scans similar to the ones shown in Fig. 8(a). At low temperatures the integrated intensity is dominated by scattering from excitations that correspond to spin waves and is expected to vary linearly with temperature.[27,12] At temperatures close to and above T_N the situation becomes complicated as the scattering can be from excitations in the 2D ordered state or more isotropic (XY or 2D Heisenberg) states.[12] The integrated intensity in Fig. 8(b) does not seem to be sensitive to the 3D ordering at T_N, but it clearly indicates that the system possesses magnetic fluctuations above T_N and even above T_{co}.

C. Magnetization and magnetic susceptibility

Magnetization measurements versus applied magnetic field, $M(H)$, and versus temperature, $M(T)/H$, were carried out on 37 mg of polycrystalline $Ca_2CuO_2Cl_2$ using a Quantum Design MPMS5 dc magnetometer. Prior to each H and T scan, the sample was heated to 400 K and the magnetic field quenched to reduced potential hysteretic effects on the internal magnetic spin arrangement.

The isothermal $M(H)$ data in Fig. 9 are nearly linear except for the 5 K data, which have a negative curvature expected for a paramagnet at low temperatures. The data between 25 and 200 K show a slight positive curvature which requires further investigation. This linear behavior contrasts with an obvious magnetic field induced spin-flop transition ≈0.7 kOe observed in single-crystal $Sr_2CuO_2Cl_2$ during magnetization[3] and magnetic neutron-diffraction studies.[29] The spin-flop transition in $Sr_2CuO_2Cl_2$ is expected from the collinear antiferromagnetic structure where two equivalent

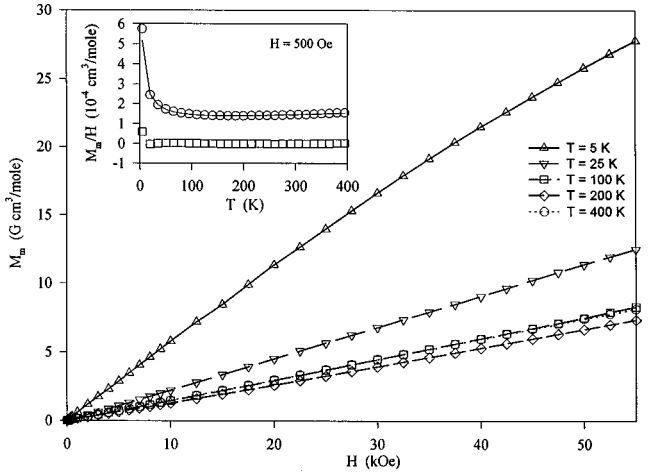

FIG. 9. Isothermal magnetization data for a polycrystalline sample of $Ca_2CuO_2Cl_2$ showing no overt sign of the spin-flop transition seen in isostructural the $Sr_2CuO_2Cl_2$ and other cuprates. The inset show the magnetization vs temperature which exhibits no obvious transitions at $T_N=247$ K. Circles are raw data, line is the calculated fit (see text), and squares are the difference.

domains are rotated by 90° with respect to one another. A similar effect should be seen in $Ca_2CuO_2Cl_2$ if it had the collinear ($\theta_0+\theta_1=0$ or π, Fig. 4, right) structure. The noncollinear ($\theta_0+\theta_1=\pm\pi/2$) helical model (Fig. 4, left) below T_N is such that the net effect of the applied magnetic field cancels out in both left- and right-handed domains (spin flop is a collective phenomena). The absence of a spin-flop transition is difficult to prove from the polycrystalline data since the transition is effectively smeared out in field due to the random particle orientations. Measurements using a single crystal will remove the uncertainty once larger samples become available.

Figure 9 (inset) shows the $M(T)/H$ data (circles) collected in an applied field of 500 Oe. The line through the circles is the fit to the data using $\chi(T)=\chi_0+C/(T-\theta)+aT$. The temperature-independent term χ_0 ($=1.04\times10^{-4}$ cm^3/mol) includes the core orbital contribution ($=-1.03\times10^{-4}$). The Curie–Weiss constants ($C=3.30\times10^{-3}$ K cm^3/mol, $\theta=-3.02$ K) are equivalent to $<1\%$ spin-$\frac{1}{2}$ impurities which are weakly interacting. The linear term ($a=1.07\times10^{-7}$ cm^3/mol K^{-1} is used to account for the tail of the cusp in the magnetic susceptibility of the 2DSLQHA expected around $J\sim1500$ K. The squares are the difference between the observed data and the fitted equation. The lack of gross features near T_N (and 300 K) is consistent with previous results for $Sr_2CuO_2Cl_2$and supports our observation that there is no orthorhombic phase transition above T_N by the absence of the cusp seen for La_2CuO_4.[30]

III. DISCUSSION

A. Magnetic scattering above T_N

The Néel temperature of the present compound, $T_N=247\pm5$ K, is well within the temperature range of T_N's of the isostructural insulating tetragonal cuprates. Due to the nonmagnetic nature of the intervening layer and large interplanar distances, very weak interplanar magnetic interactions are expected. The common scenario for the 3D AF ordering is such that *slightly* above T_N, some XY anisotropy[31,32] causes the spins to prefer an in-plane attitude and a separate, weak Ising anisotropy arises which gives the preferred in-plane spin directions. At T_N some weak interplanar interaction (see, for example, Ref. 33), magnified by the correlation length, becomes relatively important and 3D LRO occurs. We argue that the crossover of the fluctuating 2D correlated domains to a lower quasistatic spin symmetry actually occurs about 30–40 K above T_N.

If the quasistatic spin symmetry is Ising-like, then it may not be *necessary* to invoke an XY (planar) anisotropy since the planar orientation of the spins would be a consequence of the uniaxial anisotropy. Sources of Ising anisotropy are relatively limited given a square lattice model with no external symmetry-breaking perturbations. One possibility involves the quantum zero-point energy of spin waves which have been shown to produce in-plane preferred spin directions.[33,34] Alternatively, intraplanar dipolar interactions can lead to a gap in the spin-wave energy and a nonvanishing order parameter with a finite Néel temperature.[35] It can be also shown that a sufficiently large and correlated domain with spins that are all collinear but oriented in any direction on the 3D sphere will spontaneously reorient to the [110] direction under the influences of dipole-dipole interactions.[29]

B. Magnetic structure below T_N

The magnetic structure for $Ca_2CuO_2Cl_2$ proposed below T_N is another intriguing result which might deepen our understanding of the interplanar interactions. Interplanar superexchange interactions (J') are expected to be very weak in these oxyhalides because of the large interplanar spacings ($J'\propto r^{-10}$, where r is the distance between localized spins[36]) and the primarily ionic bonds in the out-of-plane direction allow little or no superexchange to occur. Even though J' cancels out in the body-centered tetragonal structure, it was shown that this degeneracy might be lifted by consideration of Coulomb exchange interactions.[33,37] The weaker biquadratic superexchange interaction is currently being examined to explain magnetic rare earth (R) ordering in some R_2CuO_4 compounds[38] and thin films of magnetic multilayer materials.[39] The biquadratic interaction goes as $\cos^2(\theta_l-\theta_{l\pm1})$ (θ_l represents the in-plane orientation of the magnetic moments in the lth CuO_2 plane) which favors a noncollinear interaction locally between neighboring planes. With the large 2D correlations inherent to these systems,[24] even weak interplanar dipole-dipole interactions[30,40] can lead to 3D ordering.[35] However, multilayer dipole-dipole calculations do not support the doubling of the c axis reported here for $Ca_2CuO_2Cl_2$. The simplest model (Fig. 4, left) with a c-axis doubling could be produced by an interaction term in the Hamiltonian which goes as $\mathbf{S}_l\times\mathbf{S}_{l+1}$. In order to resolve these issues, ongoing experiments are directed at determining the exact low-temperature spin structure.

IV. SUMMARY

Neutron-scattering and magnetization results for $Ca_2CuO_2Cl_2$ have been presented. They show that $Ca_2CuO_2Cl_2$ maintains $I4/mmm$ symmetry in the temperature range 10–300 K. Magnetic Bragg reflections indicate a

$\sqrt{2}\times\sqrt{2}\times 2$ magnetic unit cell for which we propose a general magnetic model and examine the specific cases of the collinear and helical stacking of the antiferromagnetic CuO_2 planes. The simplest model has a helical stacking arrangement of the spin planes and is consistent with the absence of a spin-flop transition in the isothermal magnetization data and with biquadratic interactions but not dipolar interactions. Elastic neutron-scattering measurements above $T_N \simeq 247$ K suggest 2D quasistatic ordering of the spin system which is consistent with either Ising-like or XY-like anisotropy below ≈ 280 K. Further studies are underway to clarify the nature and relative strengths of the anisotropic interactions and their influence on the spin behavior below and just above T_N.

ACKNOWLEDGMENTS

Stimulating discussions with F. Borsa are gratefully acknowledged. Ames Laboratory is operated for the U.S. Department of Energy by Iowa State University under Contract No. W-7405-Eng-82. The work at Ames was supported by the Director for Energy Research, Office of Basic Energy Sciences.

[1] D. C. Johnston, J. Magn. Magn. Mater. **100**, 218 (1991) and references cited therein.

[2] L. L. Miller, X. L. Wang, S. X. Wang, C. Stassis, D. C. Johnston, J. Faber, Jr., and C.-K. Loong, Phys. Rev. B **41**, 1921 (1990).

[3] D. Vaknin, S. K. Sinha, C. Stassis, L. L. Miller, and D. C. Johnston, Phys. Rev. B **41**, 1926 (1990).

[4] G. Blumberg, P. Abbemonte, M. V. Klein, W. C. Lee, D. M. Ginsberg, L. L. Miller, and A. Zibold, Phys. Rev. B **53**, R11 930 (1996).

[5] T. Imai, C. P. Slichter, K. Yoshimura, M. Katoh, and K. Kosuge, Phys. Rev. Lett. **71**, 1254 (1993).

[6] B. Keimer, N. Belk, R. J. Birgeneau, A. Cassanho, C. Y. Chen, M. Greven, M. A. Kastner, A. Aharony, Y. Endoh, R. W. Erwin, and G. Shirane, Phys. Rev. B **46**, 14 034 (1992).

[7] M. Greven, R. J. Birgeneau, Y. Endoh, M. A. Kastner, M. Matsuda, and G. Shirane, Z. Phys. B **96**, 465 (1995); M. Greven, R. J. Birgeneau, Y. Endoh, M. A. Kastner, B. Keimer, M. Matsuda, G. Shirane, and T. R. Thurston, Phys. Rev. Lett. **72**, 1096 (1994); M. Greven, R. J. Birgeneau, Y. Endoh, M. A. Kastner, B. Keimer, M. Matsuda, G. Shirane, and T. R. Thurston, Physica B **199&200**, 642 (1994).

[8] I. W. Sumarlin, J. W. Lynn, T. Chattopadhyay, S. N. Bario, D. I. Zhigunov, and J. L. Peng, Phys. Rev. B **51**, 5824 (1995), and references cited therein.

[9] S. Chakravarty, B. I. Halperin, and D. R. Nelson, Phys. Rev. Lett. **60**, 1057 (1988); S. Chakravarty, B. I. Halperin, and D. R. Nelson, Phys. Rev. B **39**, 2344 (1989); P. Hasenfratz and F. Niedermayer, Phys. Lett. B **268**, 231 (1991).

[10] H.-Q. Ding and M. S. Makivić, Phys. Rev. Lett. **64**, 1449 (1990); M. S. Makivić and H.-Q. Ding, Phys. Rev. B **43**, 3562 (1991); A. Cuccoli, V. Tognetti, R. Vaia, and P. Verrucchi, Phys. Rev. Lett. **77**, 3429 (1996).

[11] M. Corti, F. Borsa, L. L. Miller, and A. Rigamonti, J. Appl. Phys. **75**, 7146 (1994); B. J. Suh, F. Borsa, L. L. Miller, D. C. Johnston, D. R. Torgeson, and M. Corti, *ibid.* **79**, 5048 (1996); F. Borsa, M. Corti, T. Goto, A. Rigamonti, D. C. Johnston, and F. C. Chou, Phys. Rev. B **45**, 5756 (1992); B. J. Suh, F. Borsa, L. L. Miller, M. Corti, D. C. Johnston, and D. R. Torgeson, Phys. Rev. Lett. **75**, 2212 (1995).

[12] D. Vaknin, L. L. Miller, J. L. Zarestky, and D. C. Johnston, Physica C **274**, 331 (1996).

[13] Hk. Müller-Buschbaum, Angew. Chem. Int. Ed. Engl. **16**, 674 (1977).

[14] L. F. Matthiess, Phys. Rev. B **42**, 354 (1990).

[15] D. L. Novikov, A. J. Freeman, and J. M. Jorgensen, Phys. Rev. B **51**, 6675 (1995).

[16] Z. Hiroi, N. Kobayashi, and M. Takano, Nature (London) **371**, 139 (1994); T. Tatsuki, S. Adachi, M. Itoh, T. Tamura, X.-J. Wu, C.-Q. Jin, N. Koshizuka, and K. Tanabe, Physica C **255**, 61 (1995).

[17] D. Vaknin, S. K. Sinha, D. E. Moncton, D. C. Johnston, J. M. Newsam, C. R. Safinya, and H. E. King, Jr., Phys. Rev. Lett. **58**, 2802 (1987).

[18] D. Vaknin, E. Caignol, P. K. Davies, J. E. Fischer, D. C. Johnston, and D. P. Goshorn, Phys. Rev. B **39**, 9122 (1989).

[19] A. C. Larson, R. B. Von Dreele, and M. Lujan, Jr., GSAS, Generalized Structure Analysis System, Neutron Scattering Center, Los Alamos National Laboratory, CA 1990.

[20] D. Hechel and I. Felner, Physica C **235-240**, 1601 (1994).

[21] G. E. Bacon, *Neutron Diffraction* (Oxford University Press, Oxford, 1975).

[22] G. L. Squires, *Introduction to the Theory of Thermal Neutron Scattering* (Cambridge University Press, New York, 1978).

[23] D. Vaknin, J. L. Zarestky, D. C. Johnston, J. E. Schirber, and Z. Fisk, Phys. Rev. B **49**, 9057 (1994).

[24] E. Manousakis, Rev. Mod. Phys. **63**, 1 (1991) and references cited therein.

[25] Y. Endoh, K. Yamada, R. J. Birgeneau, D. R. Gabbe, H. P. Jenssen, M. A. Kastner, C. J. Peters, P. J. Picone, T. R. Thurston, J. M. Tranquada, G. Shirane, Y. Hidaka, M. Oda, Y. Enomoto, M. Suzuki, and T. Murakami, Phys. Rev. B **37**, 7443 (1988).

[26] R. J. Birgeneau, J. Skalyo, Jr., and G. Shirane, Phys. Rev. B **3**, 1736 (1971); R. J. Birgeneau, J. Als-Nielsen, and G. Shirane, *ibid.* **16**, 280 (1977).

[27] S. W. Lovesey, *Theory of Neutron Scattering from Condensed Matter* (Clarendon, Oxford, 1986), Vol. 2.

[28] R. J. Birgeneau, D. R. Gabbe, H. P. Jenssen, M. A. Kastner, P. J. Picone, T. R. Thurston, G. Shirane, Y. Endoh, M. Sato, K. Yamada, Y. Hidaka, M. Oda, Y. Enomoto, M. Suzuki, and T. Murakami, Phys. Rev. B **38**, 6614 (1988).

[29] D. Vaknin (unpublished results).

[30] T. Thio, T. R. Thurston, N. W. Preyer, P. J. Picone, M. A. Kastner, H. P. Jenssen, D. R. Gabbe, C. Y. Chen, R. J. Birgeneau, and A. Aharony, Phys. Rev. B **38**, 905 (1988).

[31] H.-Q. Ding, Phys. Rev. Lett. **68**, 1927 (1992).

[32] M. Matsuda, K. Yamada, K. Kakurai, H. Kadowaki, T. R. Thurston, Y. Endoh, Y. Hidaka, R. J. Birgeneau, M. A. Kastner, P. M. Gehring, A. H. Moudden, and G. Shirane, Phys. Rev. B **42**, 10 098 (1990).

[33] T. Yildirim, A. B. Harris, O. Entin-Wohlman, and A. Aharony, Phys. Rev. Lett. **73**, 2919 (1994); T. Yildirim, A. B. Harris, O. Entin-Wohlman, and A. Aharony, *ibid.* **72**, 3710 (1994); T.

Yildirim, A. B. Harris, A. Aharony, and O. Entin-Wohlman, Phys. Rev. B **52**, 10 239 (1995); S. Skanthakumar, J. W. Lynn, and I. W. Sumarlin, Phys. Rev. Lett. **74**, 2842 (1995); T. Yildirim, A. B. Harris, O. Entin-Wohlman, and A. Aharony, *ibid.* **74**, 2843 (1995).

[34] E. Shender, Sov. Phys. JETP **56**, 178 (1982).

[35] C. Pich and F. Schwabl, Phys. Rev. B **47**, 7957 (1993).

[36] L. J. de Jongh and A. R. Meidema, Adv. Phys. **23**, 1 (1974) and references cited therein.

[37] F. Barriquand and G. A. Sawatzky, Phys. Rev. B **50**, 16 649 (1994).

[38] V. A. Blinkin, I. M. Vitebskii, O. D. Kolotii, N. M. Lavrinenko, V. P. Seminozhenko, and V. L. Sobolev, Sov. Phys. JETP **71**, 1179 (1990).

[39] See, for example, B. Heinrich and J. F. Cochran, Adv. Phys. **42**, 523 (1993).

[40] Y. Imry, P. A. Montano, and D. Hone, Phys. Rev. B **12**, 253 (1975); D. Hone, P. A. Montano, T. Tonegawa, and Y. Imry, *ibid.* **12**, 5141 (1975).